

Quantifying the behaviour of curvature perturbations during inflation

Ellie Nelson,^{1,*} Adam J. Christopherson,² Ian Huston,¹ and Karim A. Malik¹

¹ *Astronomy Unit, School of Physics and Astronomy,
Queen Mary University of London, Mile End Road, London, E1 4NS, UK*

² *School of Physics and Astronomy, University of Nottingham, University Park, Nottingham, NG7 2RD, UK*

(Dated: July 24, 2012)

How much does the curvature perturbation change after it leaves the horizon, and when should one evaluate the power spectrum? To answer these questions we study single field inflation models numerically, and compare the evolution of different curvature perturbations from horizon crossing to the end of inflation. In particular we calculate the number of efolds it takes for the curvature perturbation at a given wavenumber to settle down to within a given fraction of their value at the end of inflation. We find that e.g. in chaotic inflation, the amplitude of the comoving and the curvature perturbation on uniform density hypersurfaces differ by up to 180 % at horizon crossing assuming the same amplitude at the end of inflation, and that it takes approximately 3 efolds for the curvature perturbation to be within 1 % of its value at the end of inflation.

PACS numbers: 98.80.Cq

arXiv:1111.6940

I. INTRODUCTION

Our understanding of the early universe has rapidly improved over the last couple of decades. Observations indicate that we live in a universe that agrees remarkably well with the cosmological standard model, a universe that is homogeneous and isotropic on the largest scales, described by the Friedmann-Robertson-Walker (FRW) spacetime and that includes cold dark matter and a cosmological constant. On smaller scales, anisotropies in the Cosmic Microwave Background (CMB) and the Large Scale Structure (LSS) are sourced by quantum fluctuations formed in scalar fields during an inflationary epoch at very early times. As the process describing the decay of these scalar fields into standard matter is not known, we map the power spectrum of the field fluctuations onto the spectrum of a conserved quantity when the size of the fluctuations is similar to the size of the Hubble radius, that is at horizon crossing, $k = aH$, (see e.g. Refs. [1, 2] for reviews of inflationary cosmology). The relative size of a given field fluctuation compared to the Hubble radius ($1/aH$) is important. Perturbations arising from fluctuations in the inflaton scalar field will become fixed, or are “frozen in”, when that scale first leaves the Hubble radius. They will be conserved while that mode is beyond the Hubble radius if mapped to a suitable quantity like a curvature perturbation, such as those discussed in the following.

Observational cosmology is entering an era in which the data from observations of LSS and the CMB are becoming much more detailed. Only eight years ago, the WMAP team were quoting cosmological parameters to an accuracy of about 10% , Ref. [3]. Now, as data sets are improving both in quality and size, the WMAP seven year observations (hereafter WMAP7) can constrain these parameters to within a couple of percent, Ref. [4]. With PLANCK we expect to do even better. Hence it is essential that the quantities we wish to study in the early universe are understood, theoretically, to this same level of precision.

It is well known that the curvature perturbations on both uniform density hypersurfaces, ζ , and on comoving hypersurfaces, \mathcal{R} , are conserved on large scales where gradient terms can be neglected (i.e. in the limit $k \rightarrow 0$) for adiabatic perturbations, Refs. [5, 6]. This result follows from the conservation of energy, Ref. [7]. The standard approach used to calculate the power spectrum of perturbations after horizon crossing assumes that the limit $k \rightarrow 0$ has been reached, see Ref. [8]. However, immediately after horizon crossing the wavenumber will not yet have become sufficiently small for this limit to be accurate and gradient terms will still play a role. In fact, in single field inflation there will still be some residual non-adiabatic pressure perturbation, δP_{nad} , present Ref. [9]. So, even in the absence of other sources of δP_{nad} , the curvature perturbation will continue to evolve for some number of efolds before settling down to its value at the end of inflation. Although it is well known that this evolution continues for a short time after horizon crossing, the exact amount of evolution has not been quantified. Exactly how long the evolution will last and how big the errors may be if the curvature perturbation is evaluated too early are issues which are yet to be

*e.nelson@qmul.ac.uk

addressed in the literature.

Much work has been done calculating the power spectra for the curvature perturbations, ζ and \mathcal{R} , during inflation (see for example Refs. [10–15] and the reviews Refs. [16, 17]). Analytic studies have to rely on either the slow roll limit, or large scale approximations, to make the calculations viable. In these limits, and without anisotropic stress, the two definitions are equal up to a sign difference e.g. Ref. [18]. In this paper we will quantify the evolution of the curvature perturbation shortly before, during and after horizon crossing. In Section IV we will demonstrate how ζ and \mathcal{R} differ at these times, how much the instantaneous horizon crossing values differ from the values at the end of inflation and how long it takes for the quantities to reach these final values.

As we do not want to rely on the slow roll approximation or the large scale limit, we solve the Klein-Gordon equations numerically, having chosen a particular scalar field potential. The linear scalar field perturbations are evolved from an initial Bunch-Davies state well inside the horizon until the inflationary expansion ends. Most of the results we present in this paper use single field chaotic inflation, the simplest single field inflation model which is in agreement with WMAP7. In order to ensure that our results are representative beyond this simplest model, we also study a set of more complicated single field models, $U = U_0 + \frac{1}{2}m^2\varphi^2$, $U = \frac{1}{4}\lambda\varphi^4$ and $U = \sigma\varphi^{2/3}$. We compare these numerical results with the standard analytic solutions for single field inflation. It is important to recognise that the analytic solution is derived using the $k \rightarrow 0$ limit but is evaluated using quantities at horizon crossing. Although this has been known in the literature for many years it is not often made clear when this mixing of late time solution and horizon crossing values is being used. In this paper we highlight the large magnitude of the inaccuracies which would result if a naïve calculation of the power spectrum at horizon crossing is performed using horizon crossing values.

Throughout this paper, although we use quantum initial conditions, we only consider the evolution of the scalar field perturbations classically. There are issues concerning how and when the quantum-to-classical transition takes place but we will not attempt to address these here. For further discussion on these issues, see for instance, Ref. [19, 20].

The paper is organised as follows. In Section II we define the relevant variables and present the relevant governing equations to determine their evolution. In the following section we detail the numerics we use to solve the equations. In Section IV we present our results, and we conclude in the final section.

II. EQUATIONS

In this section we will derive the equations for the curvature perturbation and δP_{nad} . Throughout the calculations we expand quantities into background and perturbative contributions, and shall consider scalar perturbations about a homogeneous, isotropic, FRW background model. To first order this leads to the line element

$$ds^2 = -a^2(1 + 2\phi)d\eta^2 + 2a^2B_{,i}d\eta dx^i + a^2[(1 - 2\psi)\delta_{ij} + 2E_{,ij}]dx^i dx^j, \quad (2.1)$$

where $a = a(\eta)$ is the scale factor, δ_{ij} is the flat background metric, ϕ the lapse function, and ψ the curvature perturbation, B_1 and E_1 are scalar perturbations describing the shear ($\sigma_s \equiv -B + E'$), and η is conformal time, related to coordinate time t by $a d\eta = dt$ (for details on perturbation theory see e.g. Ref. [18], the notation of which we follow where possible). Derivatives with respect to conformal time are denoted by a dash. Greek indices, μ, ν, λ , run from 0, \dots 3, while lower case Latin indices, i, j, k , run from 1, \dots 3. We shall employ the flat slicing and threading (or flat gauge) throughout this paper, where not stated otherwise.

A. Governing equations

In this paper we only consider single field inflation, which is governed by the Klein-Gordon equation, Ref. [2], in the background,

$$\varphi_0'' + 2\mathcal{H}\varphi_0' + a^2U_{,\varphi} = 0, \quad (2.2)$$

where \mathcal{H} is related to the Hubble parameter by $\mathcal{H} \equiv aH$, and prime denotes a derivative with respect to conformal time η , and the Friedmann equation,

$$\mathcal{H}^2 = \frac{1}{3M_{\text{PL}}^2} \left(\frac{1}{2}\varphi_0'^2 + a^2U_0 \right). \quad (2.3)$$

By perturbing the field and using the metric defined above in Eq. (2.1), we arrive at the perturbed evolution equation in Fourier space,

$$\delta\varphi'' + 2\mathcal{H}\delta\varphi' + k^2\delta\varphi + a^2 \left\{ U_{,\varphi\varphi} + \frac{1}{\mathcal{H}M_{\text{PL}}^2} \left(2\varphi'_0 U_{,\varphi} + \varphi_0'^2 \frac{1}{\mathcal{H}M_{\text{PL}}^2} U_0 \right) \right\} \delta\varphi = 0, \quad (2.4)$$

where we have chosen the flat gauge. Note that in flat gauge the field fluctuation is also known as the Sasaki-Mukhanov variable, Ref. [21, 22]. The Fourier component of the field fluctuation, $\delta\varphi(k^i)$, is related to the fluctuation in real space, $\delta\varphi(x^i)$, by

$$\delta\varphi(\eta, x^i) = \frac{1}{(2\pi)^3} \int d^3k \delta\varphi(k^i) e^{ik_i x^i}. \quad (2.5)$$

In order to evaluate the curvature perturbations we will need to relate the pressure, P_0 and δP , the energy density ρ_0 and $\delta\rho_1$ to the scalar field, φ_0 and $\delta\varphi_1$, by

$$P_0 = \frac{1}{2a^2} \varphi_0'^2 - U_0, \quad \rho_0 = \frac{1}{2a^2} \varphi_0'^2 + U_0, \quad (2.6)$$

and

$$\delta\rho = \frac{1}{a^2} \varphi_0' \delta\varphi' + \left(U_{,\varphi} - \frac{3\mathcal{H}}{a^2} \frac{\varphi_0'^3}{\varphi_0'^2 + 2a^2 U} \right) \delta\varphi, \quad \delta P = \frac{1}{a^2} \varphi_0' \delta\varphi' - \left(U_{,\varphi} + \frac{3\mathcal{H}}{a^2} \frac{\varphi_0'^3}{\varphi_0'^2 + 2a^2 U} \right) \delta\varphi, \quad (2.7)$$

see e.g. Ref. [18] for details.

B. Conserved quantities and δP_{nad}

As pointed out above we map the initial scalar field fluctuations, which themselves would evolve after horizon exit, onto conserved quantities, that remain constant in the limit $k \rightarrow 0$ for adiabatic perturbations. We focus here on the curvature perturbation on uniform density hypersurfaces ζ , Ref. [5], and the comoving curvature perturbation \mathcal{R} , Ref. [6]. The spectrum of the curvature perturbations can then be used to set the initial conditions for standard Boltzmann codes see e.g. Ref. [23], that are used to calculate the CMB anisotropies. The non-adiabatic pressure perturbation δP_{nad} is in general not directly observable, but is a source term for the evolution of the curvature perturbations, see Ref. [7]. Now we use the equations in the previous section above to find expressions for the curvature perturbations and the non-adiabatic pressure perturbation δP_{nad} .

The total pressure perturbation is split into an adiabatic and non-adiabatic part as Ref. [24]

$$\delta P_{\text{nad}} = \delta P - c_s^2 \delta\rho, \quad (2.8)$$

where c_s^2 is the adiabatic speed of sound and is defined as $c_s^2 \equiv P_0'/\rho_0'$. This gives us an expressions for δP_{nad} in terms of the scalar field quantities, see Ref. [25]

$$\delta P_{\text{nad}} = \left[\frac{U_{,\varphi}}{3\mathcal{H}^2 M_{\text{PL}}^2} \varphi_0'^2 - 2U_{,\varphi} \left(1 + \frac{U_{,\varphi} a^2}{3\mathcal{H} \varphi_0'} \right) \right] \delta\varphi - \frac{2U_{,\varphi}}{3\mathcal{H}} \delta\varphi'. \quad (2.9)$$

The curvature perturbation on uniform density hypersurfaces is defined as

$$-\zeta \equiv \psi + \frac{\mathcal{H}}{\rho_0'} \delta\rho, \quad (2.10)$$

which simplifies if we evaluate the right hand side in flat gauge to $-\zeta = \frac{\mathcal{H}}{\rho_0'} \delta\rho_{\text{flat}}$, where for ease of use we drop the subscript flat in the following. The comoving curvature perturbation, that is the curvature perturbation evaluated on comoving or uniform field slices, is defined by

$$\mathcal{R} \equiv \psi + \frac{\mathcal{H}}{\varphi_0'} \delta\varphi, \quad (2.11)$$

which simplifies again if the RHS is evaluated in flat gauge to $\mathcal{R} = \frac{\mathcal{H}}{\varphi'_0} \delta\varphi$. Note, that these two gauge-invariant curvature perturbations, defined in different gauges, are related by the constraint equation,

$$k^2\Psi = -9\frac{\mathcal{H}^2\varphi_0'^2}{2a^2\rho_0}(\mathcal{R} + \zeta), \quad (2.12)$$

where $\Psi = \psi + \mathcal{H}\sigma_s$ is the curvature perturbation in longitudinal gauge, that is on uniform shear hypersurfaces. As can be seen from Eq. (2.12), $\zeta + \mathcal{R}$ will become small on super-horizon scales. In the work that follows as well as studying how quickly \mathcal{R} and ζ settle to their final conserved values we will also be looking at how quickly after horizon crossing these two descriptions of the curvature perturbation agree.

Combining our results above we finally get for an arbitrary wavenumber k for a single scalar field and without imposing slow-roll in terms of the scalar field variables the non-adiabatic pressure

$$\delta P_{\text{nad}} = -\frac{2U_{,\varphi}}{3\mathcal{H}} \left[\delta\varphi' + \left(\frac{a^2 U_{,\varphi}}{\varphi'_0} + \frac{6\mathcal{H}Ua^2}{\varphi_0'^2 + 2Ua^2} \right) \delta\varphi \right], \quad (2.13)$$

and similarly the curvature perturbation on uniform density hypersurfaces,

$$\zeta = \frac{1}{3\varphi_0'^2} \left[\varphi'_0 \delta\varphi' + \left(U_{,\varphi}a^2 - 3\mathcal{H} \frac{\varphi_0'^3}{\varphi_0'^2 + 2Ua^2} \right) \delta\varphi \right], \quad (2.14)$$

and the comoving curvature perturbation, defined in Eq. (2.11), was already given in terms of the field φ .

C. Analytic Solutions

Using numerical techniques we can evaluate the expressions above at any time, analytically this is not possible. To deduce an analytic expression for the curvature perturbation, such as that used in the popular δN formalism,¹ we start from the definition [2]

$$\mathcal{P}_{\mathcal{R}}(k) = \frac{k^3}{2\pi^2} |\mathcal{R}|^2. \quad (2.16)$$

By obtaining an exact solution for power-law inflation and taking the $k \rightarrow 0$ limit, and then making an expansion about this solution, we arrive at the following, see Ref. [16]

$$\mathcal{P}_{\mathcal{R}}(k)_{\text{est}2*} = [1 - (2C + 1)\epsilon_{SR} + C\eta_{SR}]^2 \frac{a^2 H^4}{(2\pi)^2 \varphi_0'^2} \Big|_{k=aH}, \quad (2.17)$$

where $C = -2 + \ln 2 + \gamma$ and γ is the Euler constant and ϵ_{SR} and η_{SR} are slow roll parameters defined by,

$$\epsilon_{SR} \equiv \frac{3\varphi_0'^2}{2} \left[a^2 U + \frac{1}{2} \varphi_0'^2 \right]^{-1} = 2M_{\text{PL}}^2 \left(\frac{H_{,\varphi}}{H} \right)^2, \quad (2.18)$$

$$\eta_{SR} \equiv 1 - \frac{\varphi_0''}{aH\varphi'_0} = 2M_{\text{PL}}^2 \frac{H_{,\varphi\varphi}}{H}. \quad (2.19)$$

The expression given in Eq. (2.17) is only valid in the large scale limit, or equivalently a long time after horizon exit. However, it must be evaluated exactly when the corresponding mode crosses the horizon. In order to arrive at an expression which is valid at all times, we would need to consider the full analytic solution, including log corrections, see for instance Ref. [30]. We shall return to this subject in Section IV D.

¹ The δN formalism uses the direct relation of the curvature perturbation to the perturbed number of e-folds on large scales, see, for instance, Ref. [26–29]. We can relate the linearly perturbed number of expansions to the density by

$$\delta N = \frac{\partial N}{\partial \rho} \delta \rho + \frac{1}{2} \frac{\partial^2 N}{\partial \rho^2} \delta \rho^2 + \dots \quad (2.15)$$

The above result holds, to the lowest order in slow roll, for any general potential and if the slow roll parameters are assumed to be very small this simplifies to

$$\mathcal{P}_{\mathcal{R}}(k)_{\text{est1*}} = \frac{a^2 H^4}{(2\pi)^2 \varphi_0'^2} \Big|_{k=aH}. \quad (2.20)$$

For further discussions on the analytic treatment of curvature perturbations close to Horizon crossing, see for example Ref. [31, 32]

III. NUMERICAL SETUP

To set up the numerical system we have followed the work done by Salopek et al. Ref. [33]. We select a finite range of k modes which will cover all the modes which have been observed in the CMB. The WMAP team have released results corresponding to the range $k \in [3.5 \times 10^{-4}, 0.12] \text{ Mpc}^{-1}$ so we will consider a similar range below. We use the number of efolds, $\mathcal{N} = \log(a/a_{\text{init}})$, as our time variable instead of conformal time, where a_{init} is the value of a at the start of inflation and is evaluated by setting $a = 1$ today and using the background run, assuming instantaneous reheating.

The initial conditions for the background system are selected depending on the choice of potential. For the potential $U = \frac{1}{2}m^2\varphi^2$ with $m = 6.32 \times 10^{-6} M_{\text{PL}}$, we use initial conditions $\varphi_0 = 18 M_{\text{PL}}$ and $\varphi_{0,\mathcal{N}} = -0.1 M_{\text{PL}}$, see Ref. [34]. Following Ref. [33] we set the initial conditions for each k mode a few efolds before horizon crossing when the initial time $\mathcal{N}_{\text{init}}(k)$ is such that

$$\frac{k}{aH|_{\text{init}}} = 50 \quad (3.1)$$

At early times we assume the Bunch-Davies vacuum and we get the following initial conditions for modes well inside the horizon, see Ref. [33–35]:

$$\begin{aligned} \delta\varphi|_{\text{init}} &= \frac{1}{aM_{\text{PL}}\sqrt{2k}} e^{-ik\eta}, \\ \delta\varphi_{,\mathcal{N}}|_{\text{init}} &= -\frac{1}{aM_{\text{PL}}\sqrt{2k}} e^{-ik\eta} \left(1 + i\frac{k}{aH} \right), \end{aligned} \quad (3.2)$$

where $\eta = -(aH(1 - \epsilon_H))^{-1}$ and $\epsilon_H = -\frac{H_{,\mathcal{N}}}{H}$.

The behaviour of all the modes over the scales we consider are similar, so for clarity only k_1 , k_2 and k_3 modes, given below, have been shown on the graphs. It is worth noting that k_2 is the WMAP pivot scale.

$$k_1 = 2.77 \times 10^{-5} \text{ Mpc}^{-1} = 7.28 \times 10^{-62} M_{\text{PL}} \quad (3.3)$$

$$k_2 = 2.00 \times 10^{-3} \text{ Mpc}^{-1} = 5.25 \times 10^{-60} M_{\text{PL}} \quad (\text{WMAP}) \quad (3.4)$$

$$k_3 = 1.45 \times 10^{-1} \text{ Mpc}^{-1} = 3.80 \times 10^{-58} M_{\text{PL}} \quad (3.5)$$

The results presented below are for the potential $U = \frac{1}{2}m^2\varphi^2$ with $m = 6.32 \times 10^{-6} M_{\text{PL}}$, this value has been chosen such that $\mathcal{P}_{\mathcal{R}}(k) = 2.45 \times 10^{-9}$ at the end of inflation for the WMAP pivot scale. We also obtained results for three additional potentials, $U = U_0 + \frac{1}{2}m^2\varphi^2$, $U = \frac{1}{4}\lambda\varphi^4$ and $U = \sigma\varphi^{2/3}$, using parameters and initial conditions specified in Ref. [34, 35]. All the numerical results have been verified with a second numerical program to ensure their accuracy, see Ref. [36].

IV. RESULTS

Having setup the governing equations and the numerical formalism in the previous sections, we can now turn to answering the questions we raised in the introduction. Here we present our results which quantify the difference between ζ and \mathcal{R} , the magnitude of error incurred if we would use Eq. (2.16) evaluated at horizon crossing instead of Eq. (2.17), and the length of time taken for the power spectra to settle to their values at the end of inflation.

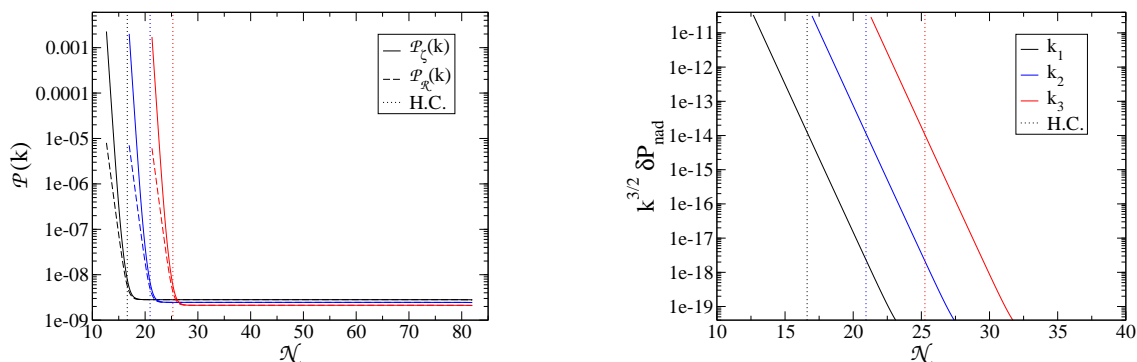
Before discussing our results in detail it is worth considering the evolution of the power spectra in general. The evolution, or indeed conservation, of the curvature perturbations has been studied in detail in the past, see Ref.

[5–7, 37] and, as expected, we find that some time shortly after horizon crossing there is no longer any appreciable evolution in either the power spectrum of ζ , $\mathcal{P}_\zeta(k)$ or the power spectrum of \mathcal{R} , $\mathcal{P}_\mathcal{R}(k)$, see Fig. 1(a). The values of these power spectra converge very quickly onto the same conserved value. This behaviour is also supported by the second graph in Fig. 1(b) which shows the non-adiabatic pressure perturbation, δP_{nad} . We find, again as expected, that during and after horizon crossing the size of δP_{nad} drops sharply towards zero. The non-adiabatic pressure perturbation is directly related to the curvature perturbation (on large scales), see Ref. [7, 37]

$$\zeta' \propto \delta P_{\text{nad}}, \quad (4.1)$$

and hence the rapid decrease in the non-adiabatic pressure perturbation causes the curvature perturbations to settle onto a conserved value.

However, it can also be seen from Fig. 1(a) that there is some evolution of the power spectra immediately after horizon crossing. This is well known in the literature where the phrase ‘soon after horizon crossing’ is commonly used to refer to the time at which the power spectra have settled down. In the sections that follow we will be looking at this evolution in more detail and in particular quantifying exactly how soon after horizon crossing the power spectra reach the final value and how different this is to the horizon crossing values.



(a) The evolution of the power spectrum of ζ , $\mathcal{P}_\zeta(k)$ and \mathcal{R} , $\mathcal{P}_\mathcal{R}(k)$ is plotted against the number of e-folds, \mathcal{N} . Both power spectra stop evolving shortly after horizon crossing, however a short period of evolution immediately after horizon crossing is visible as is a difference between $\mathcal{P}_\zeta(k)$ and $\mathcal{P}_\mathcal{R}(k)$.

(b) The evolution of δP_{nad} is plotted against the number of e-folds, \mathcal{N} . δP_{nad} rapidly drops towards zero after horizon crossing. We apply a cut off to the graph at 10^{-20} , beneath which numerical noise dominates.

FIG. 1: Both the graphs above are plotted for three different k modes. The black line (left) is k_1 , the blue line (middle) is k_2 , the WMAP pivot scale, and the red line (right) is k_3 .

A. How do ζ and \mathcal{R} differ?

The curvature perturbation on uniform density hypersurfaces, ζ and the comoving curvature perturbation, \mathcal{R} are often used interchangeably. Although they have different definitions, see Eq. (2.10) and Eq. (2.11), it is well known that on large scales they are equivalent, as can be seen from Eq. (2.12). This equivalence is however only strictly true in the large scale limit, and on smaller, finite scales this is not the case. In Fig. 1(a) we see that there is a difference between the two curvature perturbations near to horizon crossing. Three different k -modes are plotted throughout their evolution, from deep within the horizon through horizon crossing (indicated by the dotted lines), until the end of inflation.

Fig. 2 shows that ζ is as much as 20% larger than \mathcal{R} at horizon crossing and remains significantly larger for at least a couple of e-folds. This highlights the importance of making explicit the choice of curvature perturbation when carrying out calculations close to horizon crossing. We also note that ζ and \mathcal{R} take slightly different amounts of time to settle down after horizon exit, as detailed in Section IV C.

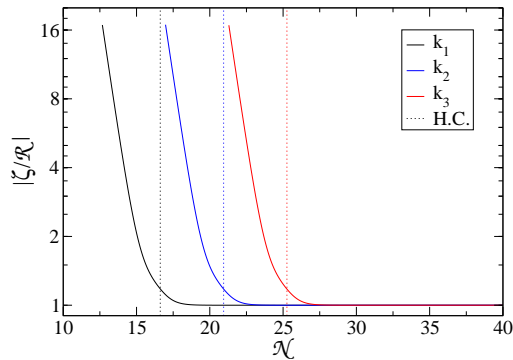


FIG. 2: The ratio of ζ and \mathcal{R} is plotted against the number of e-folds, \mathcal{N} . Evolution is visible for a short period after horizon crossing, during which time ζ is noticeably larger than \mathcal{R} . (Black line, left: k_1 , Blue line, middle: k_2 , Red line, right: k_3)

B. What is the error incurred by using horizon crossing quantities?

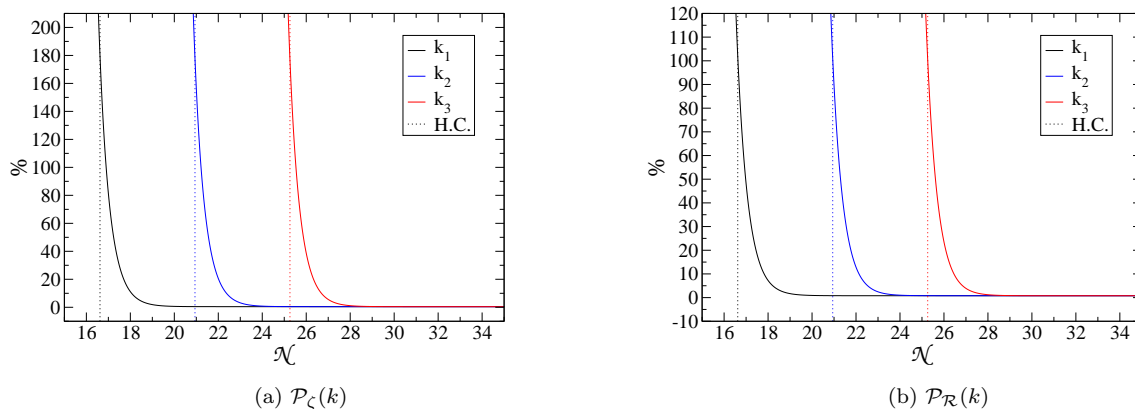


FIG. 3: The percentage difference between $\mathcal{P}(k)$ evaluated, numerically, at the end of inflation and the $\mathcal{P}(k)$ obtained at each time step. There is as much as 180% difference in the values of $\mathcal{P}_\zeta(k)$ and 100% difference in the values of $\mathcal{P}_\mathcal{R}(k)$. Both the graphs above are plotted for three different k modes. The black line (left) is k_1 , the blue line (middle) is k_2 , the WMAP pivot scale, and the red line (right) is k_3 .

As mentioned above it is well known that the values of the curvature perturbation power spectra are not the same at horizon crossing as they are at the end of inflation. However, it is not clear exactly how much of an error would be incurred if one would use the horizon crossing values instead of the correct values at the end of inflation. In Fig. 3 we can see exactly how different the power spectra are at horizon crossing compared to the values they take at the end of inflation. In Fig. 3(a) $\mathcal{P}_\mathcal{R}(k)$ is 100% larger at horizon crossing and in Fig. 3(b) $\mathcal{P}_\zeta(k)$ is 180% larger. In fact if we use an analytic approximation that does take into account the pre horizon behaviour we can see the 100% difference in the power spectra. Near horizon crossing the scalar field's wavefunction (ψ) is approximately proportional to $(1 - ik\eta)e^{ik\eta}$. At horizon crossing $|k\eta| = 1$ and $|\psi|^2 \propto |1 - ik\eta| = 2$. A few e-folds later, $|k\eta| \approx 0$ and $|\psi|^2 \propto |1| = 1$. This is a drop of 1. Hence the power spectra at horizon crossing is expected to be roughly 100% larger than that at late times. The factor of two difference in $\mathcal{P}_\mathcal{R}(k)$, has previously been found analytically, for example Ref. [19] This is, however, a large difference and might impact on calculations if $\mathcal{P}(k)_{k=aH}$ is used to approximate the value of the power spectra at the end of inflation.

C. How quickly does the power spectra reach its final value at the end of inflation?

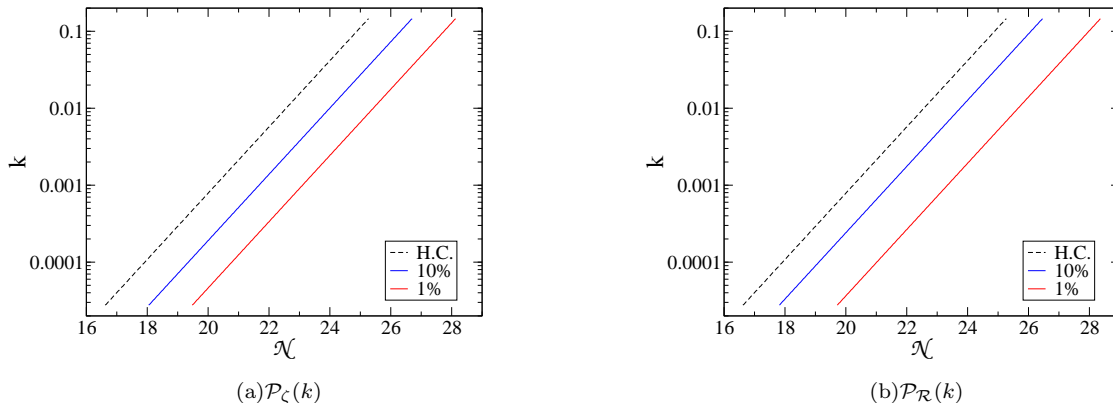


FIG. 4: These graphs show how many efolds one needs to wait for $\mathcal{P}(k)$ to be within 10% and 1% of $\mathcal{P}(k)$ at the end of inflation for a given value of k (measured in Mpc^{-1}). Note that this is independent of k . Table I gives the exact number of efolds for various potentials.

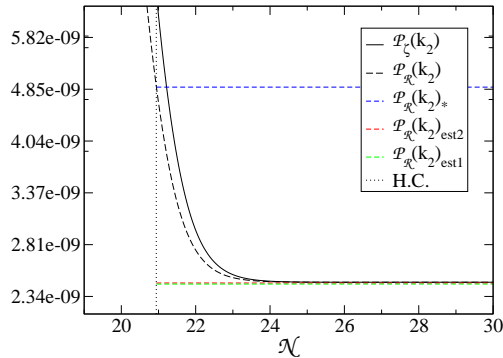
The expressions “soon after horizon crossing” and “a few efolds after horizon crossing” are often used in the literature to determine when it is reasonable to evaluate the power spectra, so that one can be confident that they have the same value as at the end of inflation. Now that we have established that the values at horizon crossing can be as much as 180% greater than those at the end of inflation we can study exactly how long after horizon crossing we must wait until the power spectra converge onto these final values. Fig. 4 shows how many efolds one needs to wait for the power spectra to be within 10% and 1% of the value they have at the end of inflation. It is clear from these graphs that this is independent of k and is in the region of “a few efolds”. Table I shows the number of efolds it takes to be within a fixed percentage of the final value, and also shows data for the three additional potentials we investigated. The choice of potential makes very little difference to the result. For every potential considered it took 1.40 – 1.44 efolds for $\mathcal{P}_\zeta(k)$ to be within 10% and 2.56 – 2.86 to be within 1%. It took 1.14 – 1.20 efolds for $\mathcal{P}_\mathcal{R}(k)$ to be within 10% and 2.30 – 3.21 efolds to be within 1%. As we highlighted in section I observational data will soon be constraining observables to within a percent, so this is at least the accuracy we would like to be able to evaluate quantities to. Our results show that to be within 1% of the correct power spectra value at the end of inflation, evaluating $\mathcal{P}_\mathcal{R}(k)$ approximately 3.2 efolds after horizon crossing and evaluating \mathcal{P}_ζ 2.9 efolds after horizon crossing, would be sufficient, for all the potentials we studied.

| | ζ | | | | \mathcal{R} | | | |
|---------------------------------|---------|------|------|------|---------------|------|------|------|
| | 10% | 5% | 3% | 1% | 10% | 5% | 3% | 1% |
| $\frac{1}{2}m^2\varphi^2$ | 1.43 | 1.80 | 2.09 | 2.86 | 1.20 | 1.59 | 1.91 | 3.10 |
| $U_0 + \frac{1}{2}m^2\varphi^2$ | 1.40 | 1.75 | 2.01 | 2.56 | 1.14 | 1.49 | 1.75 | 2.30 |
| $\frac{1}{4}\lambda\varphi^4$ | 1.44 | 1.80 | 2.08 | 2.77 | 1.18 | 1.55 | 1.84 | 2.59 |
| $\sigma\varphi^{2/3}$ | 1.41 | 1.77 | 2.05 | 2.74 | 1.20 | 1.61 | 1.98 | 3.21 |

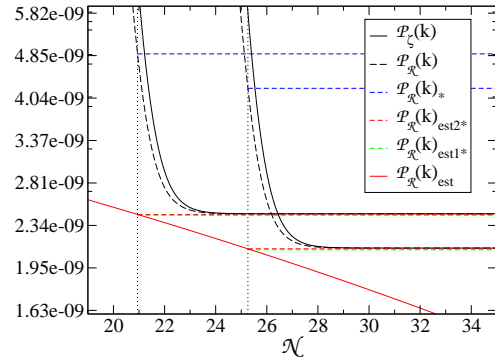
TABLE I: The values in this table represent how many efolds after horizon crossing it takes for the power spectrum to be within a fixed percentage of the power spectrum at the end of inflation.

D. Highlighting the magnitude of the error made in using the incorrect analytic expression

In most analytic calculations an expression for the power spectrum is derived using the $k \rightarrow 0$ limit but is evaluated using quantities at horizon crossing, as given in Eq. (2.17). As we mentioned in section I, it is often not made explicitly



(a) The lines in this graph are shown for the mode k_2 which is the WMAP pivot scale.



(b) The lines in this graph are shown for the mode k_2 which is the WMAP pivot scale (left hand lines) and k_3 (right hand lines).

FIG. 5: The evolution of the two types of curvature perturbation, $\mathcal{P}_{\mathcal{R}}(k)$ and $\mathcal{P}_{\zeta}(k)$ are plotted against the number of e-folds, \mathcal{N} . These numerical solutions are compared to the correct analytic solution with and without slow roll corrections (Eq. (2.17) and Eq. (2.20) and the naïve approximation of evaluating the power spectra at horizon crossing.

clear in the literature when the mixing of late time solution and horizon crossing values is being used, even when this is well understood by the authors. In Fig. 5 we compare both this correct analytic solution and the naïve calculation of the power spectrum at horizon crossing performed using horizon crossing values with the numerical solutions. In Fig. 5, as expected, the correct analytic solution gives a very good estimate to the full numerical solution. Even the analytic solution without the slow roll correction, given in Eq. (2.20), is a very good estimate to the full solution, in fact the error in not including the slow roll corrections for the WMAP scale is only a slight underestimate of 0.38%. However, when we compare the numerical solution to $\mathcal{P}_{\mathcal{R}}(k)$ evaluated at horizon crossing we find, as shown in Fig. 3(a) that there is a 100% error in our answer. As we have shown earlier in Fig. 3(b), if we evaluated the $\mathcal{P}_{\zeta}(k)$ at horizon crossing the error would be even higher at 180%, this difference in the two power spectra can be seen clearly in Fig. 5. This again highlights the importance of establishing that the correct analytic expression is used in calculations, and when different calculations and results are compared.

Another possible source of error would be to use the analytic expression given in Eq. (2.17) above, but not to evaluate it at horizon crossing. If one were to evaluate this expression ‘some e-folds after horizon crossing’, one would underestimate the amplitude of the power spectrum. This corresponds to following the red line in Fig. 5(b). For example, evaluating Eq. (2.17) 4 e-folds after horizon crossing would incur an error of 15%. Furthermore, evaluating the power spectrum at later and later times will increase the error. Lastly, it is worth noting that although the analytic and numerical expressions agree in the large scale limit, they do not agree with each other shortly after horizon crossing. As shown in the section above one must wait at least 3.2 e-folds for these two values to agree. This is particularly important if there is a second phase of evolution caused for example by a second scalar field which starts to dominate during these three e-folds, see for instance Ref. [31].

E. The Spectral Index

Using observations we can gain information about the power spectrum of curvature perturbations, which in turn allows us to constrain cosmological theories. Many observational results are given in terms of a few observables which can then be compared directly with predictions given by theories, one such observable is the spectral index. The spectral index describes the scale dependence of the power spectrum of the curvature perturbation and is defined by [2]

$$n_{\zeta} - 1 \equiv \frac{d \ln \mathcal{P}_{\zeta}(k)}{d \ln k}, \quad n_{\mathcal{R}} - 1 \equiv \frac{d \ln \mathcal{P}_{\mathcal{R}}(k)}{d \ln k}. \quad (4.2)$$

As an example of how the results presented in this paper will impact on particular observables we consider the spectral index in more detail, we present results here using chaotic inflation. Figure 6 shows, as expected, that just

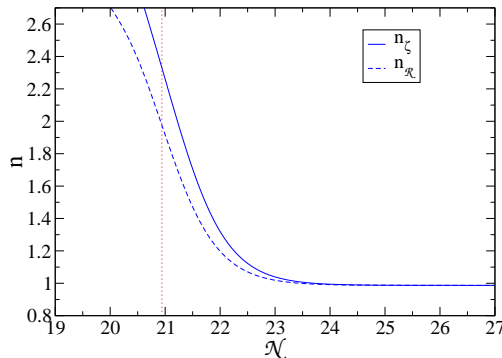


FIG. 6: The evolution of the spectral index for the two curvature perturbations, $n_{\mathcal{R}}$ and n_{ζ} , are plotted against the number of e-folds, \mathcal{N} . The lines in this graph are shown for the mode k_2 which is the WMAP pivot scale.

like the curvature perturbation the spectral index continues to evolve for a few e-folds after the mode has crossed outside the horizon. Evaluating the spectral index naively at horizon crossing gives a results of $n_{\mathcal{R}} \approx 2$ and $n_{\zeta} \approx 2.3$, which is an error in both cases of more than 100%. We find that in order for n_{ζ} and $n_{\mathcal{R}}$ to be within 1% of their values at the end of inflation, we should evaluate them at least 2.91 and 2.66 e-folds after horizon crossing, respectively. These values are similar but slightly less than the number of e-folds it takes for the power spectrum to be within 1% of it's final value, see Table 1.

V. CONCLUSIONS

In this paper we have quantified the evolution of the curvature perturbations after inflation and highlighted possible errors which can occur. As we are entering an era where we can hope to constrain cosmological parameters to within a percent using the observational data from e.g. Planck, it is of particular importance that these errors are both minimised and quantified.

After presenting the evolution equations for the scalar field, we gave the expressions for the curvature perturbations we consider. We then outlined the numerical methods used to solve these equations and gave details of the various models and the initial conditions used. In presenting our results, we found that despite ζ and \mathcal{R} being equivalent very far outside the horizon, the difference between $|\mathcal{R}|$ and $|\zeta|$ at horizon crossing can be as much as 20%. We also found the error in evaluating the power spectra numerically at horizon crossing instead of either using the correct analytic expression or the full numerical solution at late times can be as much as 180% for $\mathcal{P}_{\zeta}(k)$ and 100% for $\mathcal{P}_{\mathcal{R}}$. Lastly we showed that if one wanted to evaluate the power spectra without the use of the analytic expression Eq. (2.17), one would need to wait at least 3.2 e-folds to ensure the answer for $\mathcal{P}_{\mathcal{R}}(k)$ is correct to within 1% of the value at the end of inflation, and one would need to wait at least 2.9 e-folds to ensure the answer for \mathcal{P}_{ζ} is correct to within 1%. There was no significant difference to these results when we considered the three additional single field models presented at the end of Section III.

In this paper we point out that there is a difference between analytic and numerical expressions close to the horizon. The numerical results are the instantaneous values of the power spectrum and spectral index at horizon crossing, not the expected late time values. These instantaneous results, while not of observational significance, are useful in many ways, including as initial conditions for other analytical or numerical schemes which operate purely outside the horizon. Firstly, if we are interested in the late time values we should not take the ‘naïve’ numerical approach of evaluating these at horizon crossing. Unlike the case when using the analytic expressions these results will not be close to the correct answer. Secondly, if we are interested in the instantaneous values at or close to horizon crossing, for instance when developing codes which rely on this information, the normal analytic expressions will not give the correct answers as they are no longer valid and you need to use numerical methods.

In this paper we have only studied single field inflation models, in which the non-adiabatic pressure decays rapidly, see Fig. 1(b). This is no longer the case in multi-field systems, as a recent work has detailed, Ref. [38]. It will be interesting to repeat our analysis for more complicated models where superhorizon evolution of the curvature perturbation is expected. This would include, for instance multi-field inflation or “ultra slow roll inflation”, see for instance Ref. [14, 31]. Since in this paper we focus on the single field case, we postpone a study of these cases for

future work.

We have chosen the end of inflation as a natural end point of our calculations. After the end of inflation the inflaton is assumed to decay into the standard matter fields during reheating, the detailed mechanism of which is as yet unclear. Also, after reheating we have a multi-fluid system, and hence automatically $\delta P_{\text{nad}} \neq 0$, see Ref. [39], which means that the curvature perturbations are no longer conserved (on any scale). Consequently the values at the end of reheating might no longer be the same as those at the end of inflation.

In conclusion, we have highlighted the fact that the different curvature perturbations do evolve differently immediately after horizon exit. Confusion of the different curvature perturbations can introduce additional errors when comparing theoretical results with observations, which can easily be avoided.

Acknowledgements

We would like to thank David Seery and Will Kinney for useful comments and discussions. EN is funded by a STFC studentship. AJC is funded by the Sir Norman Lockyer Fellowship of the Royal Astronomical Society, IH is funded by the STFC under Grant ST/G002150/1, and KAM is supported in part by the STFC under Grants ST/G002150/1 and ST/H002855/1.

-
- [1] E. W. Kolb and M. S. Turner, *Front. Phys.* **69**, 1 (1990).
 - [2] A. R. Liddle and D. H. Lyth, *Cosmological inflation and large-scale structure*, CUP, Cambridge, UK (2000).
 - [3] E. Komatsu *et al.* [WMAP Collaboration], *Astrophys. J. Suppl.* **148**, 119 (2003) [astro-ph/0302223].
 - [4] E. Komatsu *et al.* [WMAP Collaboration], *Astrophys. J. Suppl.* **192**, 18 (2011) [arXiv:1001.4538 [astro-ph.CO]].
 - [5] J. M. Bardeen, P. J. Steinhardt and M. S. Turner, *Phys. Rev. D* **28**, 679 (1983).
 - [6] D. H. Lyth, *Phys. Rev. D* **31**, 1792 (1985).
 - [7] D. Wands, K. A. Malik, D. H. Lyth and A. R. Liddle, *Phys. Rev. D* **62**, 043527 (2000) [arXiv:astro-ph/0003278].
 - [8] E. J. Copeland, E. W. Kolb, A. R. Liddle and J. E. Lidsey, *Phys. Rev. D* **48**, 2529 (1993) [hep-ph/9303288].
 - [9] S. Mollerach, *Phys. Rev. D* **42**, 313 (1990).
 - [10] E. D. Stewart and D. H. Lyth, *Phys. Lett. B* **302**, 171 (1993) [gr-qc/9302019].
 - [11] I. J. Grivell and A. R. Liddle, *Phys. Rev. D* **54**, 7191 (1996) [astro-ph/9607096].
 - [12] D. H. Huang, W. B. Lin and X. M. Zhang, *Phys. Rev. D* **62**, 087302 (2000) [hep-ph/0007064].
 - [13] S. Leach, M. Sasaki, D. Wands and A. R. Liddle, *Phys. Rev. D* **64**, 023512 (2001) [astro-ph/0101406].
 - [14] S. M. Leach and A. R. Liddle, *Phys. Rev. D* **63**, 043508 (2001) [astro-ph/0010082].
 - [15] E. D. Stewart, *Phys. Rev. D* **65**, 103508 (2002) [astro-ph/0110322].
 - [16] J. E. Lidsey, A. R. Liddle, E. W. Kolb, E. J. Copeland, T. Barreiro and M. Abney, *Rev. Mod. Phys.* **69**, 373 (1997) [astro-ph/9508078].
 - [17] D. H. Lyth and A. Riotto, *Phys. Rept.* **314**, 1 (1999) [hep-ph/9807278].
 - [18] K. A. Malik and D. Wands, *Phys. Rept.* **475**, 1 (2009) [arXiv:0809.4944 [astro-ph]].
 - [19] D. Polarski and A. A. Starobinsky, *Class. Quant. Grav.* **13**, 377 (1996) [gr-qc/9504030].
 - [20] D. H. Lyth and D. Seery, *Phys. Lett. B* **662**, 309 (2008) [astro-ph/0607647].
 - [21] M. Sasaki, *Prog. Theor. Phys.* **76**, 1036 (1986).
 - [22] V. F. Mukhanov, *Sov. Phys. JETP* **67**, 1297 (1988) [*Zh. Eksp. Teor. Fiz.* **94N7**, 1 (1988)].
 - [23] A. Lewis and A. Challinor <http://camb.info/>
 - [24] H. Kodama and M. Sasaki, *Prog. Theor. Phys. Suppl.* **78**, 1 (1984).
 - [25] A. J. Christopherson and K. A. Malik, *Phys. Lett. B* **675** (2009) 159 [arXiv:0809.3518 [astro-ph]].
 - [26] A. A. Starobinsky, *Phys. Lett. B* **117**, 175 (1982).
 - [27] A. A. Starobinsky, *JETP Lett.* **42**, 152 (1985) [*Pisma Zh. Eksp. Teor. Fiz.* **42**, 124 (1985)].
 - [28] M. Sasaki and E. D. Stewart, *Prog. Theor. Phys.* **95**, 71 (1996) [arXiv:astro-ph/9507001].
 - [29] D. H. Lyth, K. A. Malik and M. Sasaki, *JCAP* **0505**, 004 (2005) [arXiv:astro-ph/0411220].
 - [30] C. Burrage, R. H. Ribeiro and D. Seery, *JCAP* **1107**, 032 (2011) [arXiv:1103.4126 [astro-ph.CO]].
 - [31] W. H. Kinney, *Phys. Rev. D* **72**, 023515 (2005) [gr-qc/0503017].
 - [32] C. T. Byrnes, S. Nurmi, G. Tasinato and D. Wands, *JCAP* **1002**, 034 (2010) [arXiv:0911.2780 [astro-ph.CO]].
 - [33] D. S. Salopek, J. R. Bond and J. M. Bardeen, *Phys. Rev. D* **40**, 1753 (1989).
 - [34] I. Huston, “*Constraining Inflationary Scenarios with Braneworld Models and Second Order Cosmological Perturbations*,” arXiv:1006.5321 [astro-ph.CO].
 - [35] I. Huston and K. A. Malik, *JCAP* **0909**, 019 (2009) [arXiv:0907.2917 [astro-ph.CO]].
 - [36] I. Huston and K. A. Malik, *JCAP* **1110**, 029 (2011) [arXiv:1103.0912 [astro-ph.CO]].
 - [37] J. Garcia-Bellido and D. Wands, *Phys. Rev. D* **53**, 5437 (1996) [astro-ph/9511029].
 - [38] I. Huston and A. J. Christopherson [arXiv:1111.6919].
 - [39] I. A. Brown, A. J. Christopherson and K. A. Malik, arXiv:1108.0639 [astro-ph.CO].